Abstract

The efficacy of urban mitigation strategies for heat and carbon emissions relies heavily on local urban characteristics. The continuous development and improvement of urban land surface models enable rather accurate assessment of the environmental impact on urban development strategies, whereas physically-based simulations remain computationally costly and time consuming, as a consequence of the complexity of urban system dynamics. Hence it is imperative to develop fast, efficient, and economic operational toolkits for urban planners to foster the design, implementation, and evaluation of urban mitigation strategies, while retaining the accuracy and robustness of physical models. In this study, we adopt a machine learning (ML) algorithm, viz. Gaussian Process Regression, to emulate the physics of heat and biogenic carbon exchange in the built environment. The ML surrogate is trained and validated on the simulation results generated by a state-of-the-art single-layer urban canopy model over a wide range of urban characteristics, showing high accuracy in capturing heat and carbon emissions. Using the validated surrogate model, we then conduct multi-objective optimization using the genetic algorithm to optimize urban design scenarios for desirable urban mitigation effects. While the use of urban greenery is found effective in mitigating both urban heat and carbon emissions, there is manifest trade-offs among ameliorating diverse urban environmental indicators.

Keyword: Carbon dioxide emission; Environmental system dynamics; Machine learning; Urban heat mitigation; Urban system planning

1 Introduction

It is projected that by 2030, approximately 5.17 billion people will live in urban areas with the expansion and densification of the built environment worldwide (UN, 2019). The extensive use of fossil fuels by densely populated cities generates concentrated emissions of anthropogenic heat, pollutants, and greenhouse gases (GHGs), leading to degraded environmental quality in urban areas. A prominent example is the phenomenon of the local warming of urban cores as compared to their rural surroundings, widely known as the urban heat island effect (UHI) (Oke, 1973, 1981). In addition, the anthropogenic stressors, especially those arising from the concentrated emissions in the built environment, have been identified as significant contributors to the long-term and emergent patterns in the global climate changes (IPCC, 2014). To mitigate the potential risks of environmental degradation by climate changes, 195 countries have committed to the long-term reduction goal set by Paris Agreement that urges each country to take the responsibility for the sustainable development of mankind (UNFCCC, 2015). Though the ambitious reduction goals and emission standards are made at the national level, it is city authorities that make most specific decisions and executions to fulfill the reduction expectations and mitigation goals (Rosenzweig et al., 2010; Bazaz et al., 2018; UNFCCC, 2020).

Among the potential mitigation strategies at city level, urban greening is proved to be effective with additional social and economic benefits. Many studies have confirmed the feasibility of urban greenery in heat (Song & Wang. 2015; Wang et al., 2016, 2018, 2019; Wong et al., 2021) and carbon emissions (Escobedo et al. 2010; Strohbach et al., 2012; Chen, 2015) via various approaches, though most conclusions were drawn from location-based observation, statistically analysis, and empirical equations (Weissert et al., 2014). Comprehensive or comparative modeling of the impact from urban greenery on heat and carbon emissions remains scarce. Moreover, conclusions from those studies varied from city to city (Weissert et al., 2014; Gao et al., 2020), depending on the urban characteristics such as native tree species, urban morphology, land use portfolio, and population (Ward et al., 2015; Velasco et al., 2016). Hence it is of pivotal importance that urban planners and policy makers should identify and create specific local strategies under a regional context, with further understanding of the environmental response under possible future scenarios, which usually requires extensive monitoring and modeling efforts. In the past decades, the development of urban observation networks and physical-based urban land surface models (ULSMs) partially fulfilled this objective, which furnishes simulations of the micrometeorological conditions at the pedestrian level in urban environment with reasonable accuracy. Some most recent ULSMs captured the dynamics of carbon dioxide (CO_2) exchange, one of the most influential GHGs, in the urban environment (Järvi et al., 2012; Goret et al., 2019; Li & Wang, 2020), enabling comparisons between physics of heat and carbon emissions and their mitigation strategies (Li and Wang, 2021a).

The use of ULSMs in urban planning and decision-making processes remains scarce hitherto: one major obstacle being the complexity of the algorithms. The guiding principle for the development of physically-based models is to capture more realistic urban dynamics at high spatiotemporal resolutions with enhanced accuracy. Hence a sophisticated ULSM inevitably evolves toward higher complexity: a typical model usually contains a group of high-dimensional non-linear functions, governing turbulent transport of mass, heat, momentum, and hydrological dynamics. ULSMs are further complicated by accounting for the interactions between diverse dynamic processes (e.g., heat and carbon). Adoption of the ULSMs by decision makers and practitioners is likely hindered by the prerequisite knowledge in physics, meteorology, hydrology, plant physiology, and programming, to interpret or adopt numerical simulation results (Pena Acosta et al., 2021).

To respond to the appeal of open science and better inform the urban planning and decision-making processes, attempts have been made to provide policy makers with e.g., operative models dedicated to decision-making with graphic or web-based programing supports (Amini Parsa et al., 2019; Sun & Grimmond, 2019). For those approaches involving urban land surface modeling, the full capability of ULSM is usually retained for better accuracy while the difficulty in operation was reduced. Nevertheless, data collection, pre-processing, calibration, and additional computational cost may continue to hamper the efforts in urban design and planning.

Machine learning (ML) techniques provide exciting opportunities to lower the barriers to using ULSMs for urban planning and decision making. ML algorithms are capable of inductively inferring complicated, nonlinear processes such as those simulated by ULSMs. Because of their strong representational power and low computational cost, they can be used as fast surrogates of computationally expensive models to facilitate parameter estimation and optimization (Cai et al., 2015; Laloy & Jacques, 2019; Kim & Boukouvala, 2020; Xu & Liang, 2021). ML-based surrogate models are particularly suitable for urban planning and decision-making applications. First, for design and planning purposes, the prediction of the general trend (such as temporally averaged CO_2 emission) is more important than detailed representation of the dynamics (such as diurnal variation). Therefore, the surrogate model can focus on emulating temporal and/or spatial statistics. The simplification reduces the level of complexity of surrogate modeling, and the ML models can be trained with a moderate amount of observations and/or simulation results of

ULSMs. Second, trained ML models typically require minimal computational cost compared to ULSMs that are computationally expensive. Third, ML models can be easily deployed in user interfaces across platforms, for example via notebook environments such as Jupyter (Executable Books Community, 2020). This enables users to access the surrogates without meeting the prerequisite of ULSMs.

Various ML algorithms have been used to build surrogate models, such as radial basis function (Akhtar & Shoemaker, 2016), deep neural networks (Gettelman et al., 2021), and Gaussian process regression (Laloy & Jacques, 2019). Among these algorithms, Gaussian process regression (GPR) is a non-parametric ML technique (Rasmussen and Williams 2006) and has been shown to perform well in various applications (e.g., Camps-Valls et al., 2018; Fang et al., 2018). Through using appropriate covariance functions such as squared exponential kernel, GPR can enforce local smoothness, which may be beneficial for searching of the optima (Razavi et al., 2012; Laloy & Jacques, 2019).

The recent decade has seen the rapid development of machine learning models primarily focused on urban heat mitigation (Gobakis et al., 2011; Oh et al., 2020; Pena Acosta et al., 2021), the interpretation of remote sensing data (Milojevic-Dupont & Creutzig, 2021), and carbon emissions (Creutzig et al., 2019; Zhang et al., 2021). Only limited effort was devoted specifically to urban planning purpose (Pena Acosta et al., 2021), focused on individual environmental processes separately. With the rapid global urbanization and climate changes, it is imperative to extend the application of ML techniques to holistic urban system dynamics which helps integrate multiple urban physics and diverse environmental impacts, and to foster sustainable urban design and planning.

To further improve the viability of ULSM and aid sustainable urban design and planning, in this study, we adopt the GPR algorithm (Rasmussen and Williams 2006) to capture the physics of thermal and CO_2 exchange, based on the state-of-the-art Arizona State University (ASU) Single-Layer Urban Canopy Model version 4.1 (ASLUM v4.1) (Li & Wang, 2020; Wang et al., 2021a). The proposed ML surrogates can effectively reduce the computational time and cost associated with physical models while maintaining the robustness and accuracy, thus helpful to new users from urban design and planning sectors who are not familiar with urban climate modeling. Meanwhile, we use multi-objective genetic algorithm (McCall, 2005) to find the optimal configurations of the urban system for simultaneous mitigation of heat and CO_2 emissions. The results will potentially enhance our understanding of the water-heat-carbon dynamics in urban ecosystem and promote the development towards sustainable cities.

2 Method

2.1 Single layer urban canopy model

Among the current ULSMs, single layer urban canopy models (SLUCMs) are probably the most widely used schemes for urban system modeling. In SLUCMs, the urban landscape is represented as a generic unit of two-dimensional (2D) street canyon, consisting of two arrays of buildings separated by a road, with infinite longitudinal dimension (Fig. 1). The morphology of urban areas is defined by the canyon aspect ratio (building height/street width, H/W), while the land cover type can be configured into different categories such as different types of pavements, vegetation, and soil. The continuous improvement of SLUCMs in the last decade enables detail modeling of thermal, hydrological, ecological, and physiological processes in urban areas (see e.g., Masson, 2000; Lemonsu et al., 2012; Yang et al., 2015a; Ryu et al., 2016; Stavropulos-

Laffaille et al., 2018; Meili et al., 2020; Wang et al., 2013, 2021a). These models have been used to assess the impacts of various characteristics of the built environment, especially the designed urban mitigation strategies, on the thermal, pollutants, and carbon emissions in cities.

In this study, we adopt the newest version of Arizona State University Urban Canopy Model (ASLUM version 4.1, Li & Wang, 2020, 2021b). ASLUM v4.1 features the coupling of urban energy and water dynamics with photosynthesis and respiration from urban vegetation, which enables us to quantify the compound environmental impact of urban mitigation strategies, urban greening in particular, for both urban heat and CO_2 mitigation.

To characterize the urban environment, the in-canyon air temperature (T_{can}) is calculated from the energy balance closure in street canyon (i.e., building walls and grounds) by (Wang et al., 2013),

$$T_{\mathrm{can}} = \frac{\frac{2H}{W}\frac{T_w}{RES_w} + \frac{f_p T_p}{RES_p} + \frac{f_v T_v}{RES_v} + \frac{f_s T_s}{RES_s} + \frac{T_a}{RES_{can}}}{\frac{2H}{W}\frac{1}{RES_w} + \frac{f_p}{RES_p} + \frac{f_v}{RES_v} + \frac{f_s}{RES_s} + \frac{1}{RES_{can}}}, \qquad (1)$$

where T and f represent the temperature and fraction of the sub-facets; RES is the aerodynamic resistance on each sub-facets; subscripts w, p, v, s, a, can denote walls, paved surfaces, vegetation, bare soil, atmosphere, and canyon respectively. In addition, the biogenic net ecosystem exchange (NEE) is given as

$$\mathrm{NEE} = R - \mathrm{GPP}, \qquad (2)$$

where R is the total respiration from soil and vegetation; GPP is the total gross primary production from trees and lawns. The value of NEE follows the convention in ecology with both R and GPP positive numbers, and negative NEE means net carbon sink.

2.2 Dataset

A simulated dataset generated by ASLUM v4.1 are used for the subsequent ML emulations. To improve the robustness of ML models over a wide range of urban configurations, we conduct a large number of numerical simulations (N = 55388) by ASLUM v4.1 using a variety of critical system design parameters. Training ML models only requires a small portion of the dataset, while the majority of the dataset will be used in model testing and evaluation (see Section 3.1). Each simulation is driven by in-situ observation from an eddy covariance (EC) system in west Phoenix, Arizona (33.483847ºN,112.142609ºW) as the meteorological forcing. The EC system measured basic meteorological variables and energy fluxes at 22 m above the ground (>15 m above average roof level). Data retrieved from this EC tower (Chow, 2017) has been used in previous urban studies ranging from surface energy dynamics, urban environment modeling, and boundary layer physics (Chow et al., 2014; Song et al., 2017; Meili et al., 2020). The meteorological forcing used in subsequent simulations includes the downwelling shortwave and longwave radiation, atmospheric temperature, pressure, humidity, and wind speed (Fig. 2). We selected 24 hours of measurement during a typical clear day in early summer (May 11th, 2012) to drive the physical model, with air temperature of 35 ºC at the maximum and 23 ºC at the minimum. Meanwhile, the time selection of meteorological forcing avoids the influence from random weather events like the presence of cloud, precipitation, and cold/heat waves. During the simulation period, ALSUM v4.1 predicts the evolution of upwelling radiation, surface temperatures and heat fluxes, and biogenic CO_2 at an interval of 5 minutes, and aggerates these variables into to 30-minutes average as the outputs.

The scenarios of urban system design in ASLUM v4.1 are represented by several groups of parameters, including the street morphology, thermodynamic properties of urban fabric, urban greenery properties, overall land use types, and landscaping management schemes. Previous studies have shown that certain parameters of the ASLUM v4.1 possess higher sensitivity especially in prediction of extreme events and design optimization. These parameters are hereafter referred to as the critical design parameters (Yang & Wang, 2014; Yang et al., 2016; Li & Wang, 2021b). In the light of previous studies, here we select 24 urban system critical design parameters in four groups that are most impactful to the urban thermal environment and carbon exchange dynamics (Table 1). The 24 design parameters are sampled from individually prescribed probability distribution functions (PDFs) (see details in Table 1 in Li & Wang, 2021b), respectively, and are considered to be independent. The possible covariances among different parameters, in particular the soil thermal and hydrological properties, have insignificant impact on the output of ASLUM (Wang et al., 2011). The PDFs of design parameters are primarily derived from field or laboratory measurements, reported values from literature, or best estimates within the physical ranges (Li & Wang, 2021b). In each simulation, we monitor the mean air temperature at the pedestrian level inside of street canyon (T_{can}), and the mean net ecosystem exchange (NEE) over the street canyon. Finally, all simulations are randomly split into two sets (training and test) for the subsequent ML regression and optimization.

2.3 Gaussian process regression

GPR is a Bayesian kernel regression method that uses a Gaussian Process (GP) to describe the distribution of the quantity of interest and the Bayes' theorem to infer the posterior distribution (Rasmussen and Williams 2006). A GP refers to a set of random variables, $\{Y_1, Y_2, \ldots, Y_k\}$ (often indexed by inputs), that jointly follow a multivariate Gaussian distribution. GPR starts by specifying the prior (i.e., before seeing any data) mean and covariance of the joint

Gaussian distribution using the mean function $\mu(\mathbf{x}) = E[Y(\mathbf{x})]$ and a covariance function $k(\mathbf{x},\mathbf{x}') = E[[Y(\mathbf{x}) - \mu(\mathbf{x})][Y(\mathbf{x}') - \mu(\mathbf{x}')]]$, respectively. Here, $\mathbf{x}$ is a d-dimensional vector and may include space coordinates, time, or controlling variables of Y. The mean and covariance functions should reflect the prior knowledge of the general trend and level of smoothness of the target function, respectively. The covariance implicitly maps the inputs to features $\phi(\mathbf{x})$. By doing so, GPR can approximate complex, nonlinear relationships between the target ($Y = T_{\mathrm{can}}$ or NEE) and inputs (sampled from the ASLUM v4.1 parameter space).

Once training data are introduced, GPR uses the Bayes' Theorem to infer the posterior distribution of the target. Let $D = \{(\mathbf{x}_1, y_1), (\mathbf{x}_2, y_2), ..., (\mathbf{x}_n, y_n)\}$ denote training data, the posterior distribution of the target variable at an unseen data point, $Y^* = Y(\mathbf{x}^*)$ is given by:

$$Y^* \mid D, \mathbf{x}^* \sim N(\overline{y}^*, Var(Y^*)) . \tag{3}$$

The posterior mean and variance are given below:

$$\overline{y}^* = \mu(\mathbf{x}^*) + \Sigma^{*T}(\Sigma + \sigma_\varepsilon^2 I_n)^{-1}[\mathbf{y} - \mu(\mathbf{x})] , \tag{4}$$

$$Var(Y^*) = \sigma_0^2 - \Sigma^{*T}(\Sigma + \sigma_\varepsilon^2 I_n)^{-1}\Sigma^* . \tag{5}$$

In the above equations, $\mathbf{y} = \{y_1, y_2, ..., y_n\}$, σ_ε^2 is noise variance, σ_0^2 is signal variance, a hyperparameter of the covariance function, Σ denotes the prior covariance matrix of the training data with its *ij*-th entry as $\Sigma_{i,j} = k(\mathbf{x}_i, \mathbf{x}_j)$, and Σ^* is a vector denoting the covariance between training and test data, i.e., $\Sigma_i = k(\mathbf{x}_i, \mathbf{x}^*)$.

In this study, we use GPR to construct surrogate models for NEE and T_{can}, respectively. Both surrogate models use the critical design parameters of the ASLUM as input variables after scaling to [0, 1]. We note that this is a high dimensional problem with 24 input variables (p = 24), which would pose challenges for some commonly used surrogate modeling techniques such as polynomial chaos expansion (He et al., 2020). For both surrogate models, we specify a linear prior mean and the commonly used squared exponential covariance function. The models are trained using simulation results of ASLUM v4.1 described in Section 2.2. The two hyperparameters of the covariance function (signal variance and range) are tuned by maximizing log likelihood; the other hyperparameters (noise variance and coefficients of the linear mean function) are estimated once the best signal variance and range are determined. In particular, the signal variance and range (λ) of the covariance function, noise variance, and coefficients of the linear mean function (β) are estimated by maximizing the log marginal likelihood as a function of these hyperparameters (Rasmussen and Williams 2006):

$$\begin{aligned}\log P\left(\mathbf{y}\middle|X,\beta,\lambda,\sigma_f^2,\sigma_n^2\right) = &-\frac{1}{2}(\mathbf{y}-H\beta)^T\left[\sum\left(\sigma_0^2,\lambda\right)+\sigma_n^2 I_n\right]^{-1}(\mathbf{y}-H\beta) \\ &-\frac{n}{2}\log 2\pi-\frac{1}{2}\log\left|\sum\left(\sigma_0^2,\lambda\right)+\sigma_n^2 I_n\right|\end{aligned}, \quad (6)$$

where $X=\left[\mathbf{x}_1^T,...,\mathbf{x}_n^T\right]$, $H=\left[\mathbf{1}_n,X\right]$, and $\mathbf{1}_n$ denotes a column vector of ones. Hyperparameters that maximize the above log marginal likelihood was identified using a quasi-Newton method. This is more computationally efficient than methods such as grid search because the overhead of calculating the derivatives is small (Rasmussen and Williams 2006).

The model trained using the selected hyperparameters is then used for optimization (Section 2.4). In this study, we use the posterior mean $\bar{y}^*$ to emulate temporally aggregated NEE and T_{can} simulated by ALSUM. However, whenever needed it is possible to use the posterior variance with stochastic/robust optimization techniques (e.g., Diwekar, 2020; Mishra et al., 2020).

Besides GPR, we also use the radial basis function (RBF) interpolation technique (McDonald et al., 2007) to construct the surrogates. RBF interpolation constructs an exact emulator; in other words, the fitted function is exactly equal to the target variable at training data points. Because of this appealing feature and satisfactory performance of RBF in previous studies (Akhtar & Shoemaker, 2016), we include RFB interpolation in this study to construct surrogates for T_{can} and NEE, respectively. The Gaussian basis is used, and its decay rate hyperparameter was selected by maximizing coefficient of determination on a validation set separate from training data.

2.4 Metrics of environmental quality and multi-objective optimization

As mentioned, we use daily mean in-canyon temperature (T_{can}) and biogenic NEE to represent thermal and carbon environment in this study. During summertime, both lower T_{can} and NEE are preferred for better heat mitigation and CO_2 reduction purposes. It is noteworthy that urban mitigation strategies will affect the behavior of CO_2 exchange over vegetated surfaces, primarily by affecting the atmospheric temperature and radiation redistribution. Specifically, the shading effect of tall urban trees (Wang, 2014; Upreti & Wang, 2017) reduces photosynthetic active radiation on understory lawns, lowering CO_2 uptake rate. Meanwhile, the cooling effect caused by shading and evapotranspiration from green spaces reduces enzyme activities in photosynthesis and respiration processes, weakening CO_2 uptake and release at the same time. The complex interactions between heat and biogenic carbon dynamics make it difficult to disentangle the effect of mitigating heat and CO_2 emissions separately.

To account for the compound mitigation effect to heat and carbon emissions, we perform multi-objective optimization to minimize T_{can} and NEE simultaneously. The decision variables (24 ASLUM v4.1 parameters) are constrained by their physically feasible ranges (Table 1). The optimization problem is solved by an elitist genetic algorithm (Deb, 2001) in MatLab®. A population size of 500 is used in each generation with the maximum of 500 generations when searching for the Pareto solutions. Mathematically, Pareto solutions are defined as a compromise to "no other solution that can improve at least one of the objectives without degradation any other objective" (Ngatchou et al., 2005). The optimization process stops when the movement of the points on the Pareto front between the final two iterations is small.

To facilitate the assessment of optimization results and to enable direct comparison among designed scenarios, we introduce a compound heat-carbon index (CHCI):

$$\mathrm{CHCI} = \alpha \overline{T_{\mathrm{can}}} + (1-\alpha)\overline{\mathrm{NEE}}, \tag{7}$$

where $0 < \alpha < 1$ is the weight of multiple environmental indicators (for simplicity, we use α = 0.5 for subsequent analysis), and the overhead bar denotes the normalization by

$$\overline{X} = \frac{X - X_{\min}}{X_{\max} - X_{\min}}, \tag{8}$$

with X being T_{can} or NEE. Qualitatively, lower CHCI represents lower temperature and stronger carbon sink, thus indicates better overall environmental quality. Based on the simulated dataset, the values of $T_{can,max}$, $T_{can,min}$, NEE_{max}, and NEE_{min} in this study are 39.77 ºC, 8.47 ºC, 0.090 mg $m^{-2}s^{-1}$, and –0.190 mg $m^{-2}s^{-1}$, respectively.

3 Results and Discussion

3.1 Machine learning surrogates

In this study, we train two GPR models to emulate T_{can} and NEE, respectively, using 5% of the simulated dataset (N_{train} = 0.05N = 2769), as described in Section 2.2. We then evaluate the emulation accuracy of the two surrogates on the test data (N_{test} = 0.95N = 52619). Figure 3ab shows the comparison between T_{can} and NEE simulated by the physical model ASLUM v4.1 and ML surrogates on the test data. For each scenario, CHCI is calculated by Eq.(6) using normalized

T_{can} and NEE from ASLUM and GPR models respectively (Fig. 3c). The result shows GPR models reproduce the environmental metrics with satisfactory accuracy, with coefficient of determination (R^2) above 0.96 for T_{can}, NEE, and CHCI. Figure 3d shows the change of R^2 and normalized root mean square errors ($RMSE_n$) of the comparisons when varying the training sample size from 0.5% to 10% with 0.5% increment ($0.005N = 277$). R^2 and $RMSE_n$ shown in Fig. 3d are the ensemble means from 20 runs with different random seeds to reduce the influence of data heterogeneity and randomness in training sample selection. The variations among 20 runs are insignificant with the coefficient of variance (standard deviation / mean) smaller than 0.002 for R^2 and 0.02 for $RMSE_n$. Generally, the model performance improves with the increase of training sample size, but the change becomes marginal when sample size is greater than 3% ($0.03N = 1662$). The GPR surrogate models retain reasonable accuracy ($R^2 > 0.90$ for T_{can} and NEE on test data) when trained by only 0.5% (277) of the dataset while tested on the rest. Small training sample size can potentially cause over-fitting, especially for models fitting on a large number of input features due to the "curse of dimensionality" (Bessa et al., 2017). In this study, the minimum training sample size required to avoid over-fitting issue is around 0.3% ($0.003N = 166$), but the model performance and stability degrade significantly on test samples when training sample size is smaller than 0.5% of the dataset. Users with a limited amount of data points from observations should be cautious about the over-fitting issue and employ strategies such as reducing the input dimension and model averaging (Cawley and Talbot, 2007, 2010). To the extent allowed by computational budget, we suggest increasing training sample size to ensure better and more robust model performance.

The emulation accuracy of RBF interpolant is substantially lower than GPR ($R^2 = 0.77$ and 0.88 for T_{can} and NEE, respectively, evaluated on test data). Therefore, we did not use the

RBF surrogates for optimization. A possible cause of the inferior performance is that RBF may be subject to numerical stability and robustness issues with large datasets (Skala, 2017). However, RBF may be an attractive candidate for surrogate modeling when only a small amount of training data is available (Razavi et al., 2012; Akhtar & Shoemaker, 2016).

In addition to the satisfactory accuracy, our performance benchmark shows that the GPR surrogate models only take 3.6, 17.6, and 35.0 seconds to simulate a group of 10, 50, and 100 different scenarios respectively, which is eight times faster on average than ASLUM v4.1 (tested on Intel Xeon E-2186G 3.8GHz with 12 logic cores and 40GB RAM). The high efficiency reduces the time cost of calculation, facilitating decision making processes and enabling fast comparison between a large amount of scenarios, especially when exhaustive search for best case is desired. The improvement in calculation efficiency also promotes fast assessment of variable sensitivity for high-dimensional physical-based ASLUM v4.1, in comparison with the previous sensitivity analysis (Li & Wang, 2021b).

3.2 Multi-objective optimization

Once the GPR emulations of ASLUM v4.1 is trained and tested, we use a multi-objective genetic algorithm (GA) optimization process to find the desirable urban system design within the physically feasible range of the critical design parameters in Table 1. The multi-objective GA finds urban configurations that minimize T_{can} and NEE simultaneously, leading to Pareto solutions. The Pareto solutions characterize the trade-off among multiple objectives in a constrained optimization. In this study, a tradeoff exists between the two urban environmental measures, viz., T_{can} and NEE, because photosynthesis shrinks with temperature decrease, though the underlying mechanisms are much more complex. Figure 4 shows the comparison of results of

ASLUM v4.1 simulations and the Pareto front formed by multiple Pareto solutions (n = 134) identified by GA with similar CHCI but different combinations of T_{can} and NEE. The Pareto solutions are located lower left corner, within the range of CHCI from −0.05 to 0.10. Overall, the CHCI values of the Pareto solutions are significantly lower than the training and test dataset, indicating the potential further improvement of environmental quality via optimized urban design.

Furthermore, the Pareto front roughly consists of two segments: the upper left wing running parallel with the equi-CHCI contours and the lower right tail with increasing CHCI. The segment of Pareto front with (roughly) constant CHCI can be physically interpretated as that the optimal urban designs for mitigating carbon emission can be obtained with the trade-off of compromising heat mitigation. Yet, the total efficacy of the combined benefit of carbon-heat mitigation is achieved with constant CHCI. The lower right tail, in contrast, signals that if urban system design put more weight on the cooling effect, as a consequence, the objective of carbon emissions will be strongly degraded. This is manifested in that the right tail extends in the direction where CHCI increases, meaning the combined benefit of carbon-heat mitigation will be severely hampered: only marginal cooling effect can be obtained at the expense of significant increases in carbon emission.

Note that here we only consider two essential measures of urban environmental quality. If more environmental metrics are to be included (e.g., health risks of urban residents due to degraded thermal/air quality), the multi-objective optimization will likely produce smaller (due to more optimization constraints) solution domain with lowest CHCI as the candidate for urban system design. But the trade-offs among diverse environmental indicators will remain the guiding principles for researchers and policy makers to design and assess more livable cities using multi-objective optimization.

3.3 Implications to urban system design

For optimal urban system design, one would seek for the urban characteristics that lead to Pareto solutions. The deviations of these parameters from their *status quo* values indicate the potential urban system design for planners to ammolite the thermal and carbon environments in cities. Figure 5a shows the histograms of initial and optimized (Pareto solutions) distributions of the 24 critical design parameters. Among the Pareto solutions (n = 134), we found that the key parameters shared similar values skewed to the edge of prescribed boundaries from Table 1. Overall, wide street (W), low-rise building (H), high vegetation coverage (f_v), dense lawns (LAI_G), and small bare soil fraction (f_s) are most likely to furnish Pareto solutions for thermal and carbon mitigations. To achieve desirable environmental benefits, these urban features need to fall within a small range (Fig. 5b). Good environmental performance is also associated with high trees (h_T) with large crown (r_T) and dense canopy (LAI_T). Environmental responses (i.e., T_{can} and NEE) are not sensitive to parameters related to trees than those related to urban street morphology and land use, yet tree parameters play important roles affecting both heat and CO_2 exchanges in urban environment (Li & Wang, 2021a). As a result of heat mitigation, urban greenery saves building energy consumption during summertime, indirectly reducing CO_2 emissions induced by fossil fuel power generation (Akbari, 2002). This study only considers biogenic CO_2 exchange. The importance of greenery-related urban features (i.e., f_v, f_s, LAI_G, LAI_T, h_T, r_T, etc.) might be more substantial if point source emissions from fossil fuel power plants are included.

Unlike the parameters of street canyon geometry and plant properties, no significant skewness of material properties of pavement and building materials are observed, except for the albedo of vegetated ground (aG_3) and heat capacity (cW_1) and thermal conductivity (kW_1) of building walls. Albedo of vegetated ground (aG_3) directly affects the energy flux and the skin temperature of ground vegetation (i.e., urban lawns) and controls the rates of evapotranspiration, photosynthesis, and respiration. Active evapotranspiration dissipates surface energy via latent heat (Yang & Wang, 2017; Aram et al., 2019), triggering changes in the ambient temperature and further altering biogenic CO_2 exchanges through physiological processes. In addition, thermal properties of building walls regulate the energy exchange rate between building and canyon atmosphere, more effectively than roofs, especially if the building interior thermal environment is regulated by the operation of heating, ventilation, and air conditioning (HVAC) systems or effective (green) building energy designs (Wang et al., 2021b).

It is noteworthy that initial soil moisture (SWCi) shows limited sensitivity with the optimal mean nearly identical to its initial value (Fig. 5b). In urban environment, scheduled irrigation controls soil moisture, therefore the optimal irrigation amount exists corresponding to the optimal soil moisture. The finding is consistence with Li and Wang (2021a), where it is found that excessive irrigation may not help to mitigate carbon emission. This is due to the fact that the extra moisture can promote soil respiration (hence increase carbon emission), whereas the marginal cooling due to extra irrigation is not significant. This effect has been corroborated by Vivoni et al. (2020), based on a year-long in-situ measurement at a desert urban park, and was referred to as an "oasis effect" of urban irrigation that enhances evapotranspiration and CO_2 exchanges. It is also noteworthy that the tail observed in the Pareto front in Fig. 4 with degraded co-benefit of heat and carbon mitigation can be largely attributed to this effect as well.

Overall, the good agreement between the results of the GA multi-objective optimization and previous physically-based simulations (Li & Wang, 2021a) underlines the reliability and fidelity of the ML surrogates in the current study. Results show that specific urban system design strategies for effective mitigation of heat and carbon emissions include more urban green spaces, choices of urban vegetation types, meticulous management of irrigation schedule, and adoption of smart building and pavement materials. The ML-based surrogates and optimization algorithms can be used in the place of physical models with significantly reduced complexity and computational cost, and furnish excellent operative models for fast decision making. Nevertheless, as revealed by this study, it is of critical importance to re-iterate here that multi-objective optimizations are intrinsically constrained by the competing interest among diverse objectives. Furthermore, the GA optimization method in this study helps to inform policy makers and practitioners at the onset of planning stage, and to gauge their preference of specific or compound design objectives, e.g., improvement of thermal comfort, air quality, building energy efficiency, or reduction of health risks, etc.

3.4 Future development

This study aims to provide a practical toolkit to design and evaluate the impact of urban characteristics on improving the livability of urban environment, based on ML surrogates trained on a simulated dataset. We adopt GPR in our applications to showcase the performance of ML emulation in terms of model accuracy and stability. However, many other popular ML or deep learning algorithms, such as Random Forest, support vector machine, or deep neural networks, can be adopted for urban system design depending on specific applications or the user preference. For example, support vector machine with RBF kernel is expected to outperform GPR when training data is scarce (Razavi et al., 2012; Akhtar & Shoemaker, 2016).

The design optimization in this study is primarily based on ML models without the aid from physically-based UCM. Theoretically, ML emulations are expected to be more accurate within the range of training data than when it is used for extrapolation. This caveat will be relaxed by adaptive learning with dataset continuously retrieved from observation or numerical modeling to retrain the ML models during optimization. Adaptive learning could further improve the model accuracy and optimization performance but might sacrifice model simplicity and practicality for non-machine learners (i.e., urban planner/designers and decision makers).

In this study, we focus on heat and carbon emissions as the indicator of the urban environmental quality. Though they are the major concerns amid the global climate change, many other factors affect the comfort and health of urban dwellers that should be considered in sustainable urban development. For example, relative humidity and thermal radiation (i.e., ultraviolet, UV) play important roles in human thermal comfort and their influence varies among climate regions (Abdel-Ghany et al., 2013; Baruti et al., 2019). Thermal discomfort caused by undesired relative humidity and excessive UV exposure can be mitigated by proper urban designs of urban geometry, building and pavement materials, green and blue spaces (Lai et al., 2019). Moreover, air pollutions such as high levels of ozone and particulate matters (PM) concentration can be alleviated by street trees, though the mitigation effect is highly dependent on tree location and species (Barwise & Kumar, 2020) and requires dedicated tree models to quantify (Riondato et al., 2020). As shown by the Pareto solutions in Fig. 4, exclusive urban planning objectives, such as UHI mitigation by reflective pavements, often lead to severe compromise of other environmental qualities (e.g., carbon emissions). Such one-sidedness in urban planning strategies has practically gained upper hand in policies of some local municipalities, which leads to many unintended physical consequences in the real world (Yang et al., 2015b). It is important that urban practitioners bear in mind the potential trade-offs of multi-objective designs, and more sustainable urban planning strategies should account for the interactions of total urban system dynamics, instead of trying to "optimize" for singular environmental indicators (in particular, heat mitigation).

Furthermore, the high computational efficiency of ML emulation can enhance the performance and predictive capacity of regional urban hydroclimate modeling by serving as surrogates of multi-scale numerical platforms such as the widely-used Weather Research and Forecast (WRF) model (Skamarock et al., 2019). Currently, WRF resolves urban land surface using WRF-UCM coupling framework, which allows simple configuration of urban characteristics with limited urban types. Comparing to the simplified UCM in WRF model, ML models learned from full version of UCM will produce more detailed and accurate results with much improved computational economy. As cities are more vulnerable in climate change than other nature areas, the improvement in computation speed and accuracy are not trivial in terms of the sustainable development of the human society.

4 Concluding remarks

This paper presents a method emulating a complex urban land surface model using machine learning, aiding the direct interpretation of modeling results for urban planners and policymakers who might have less knowledge on urban land surface models and computing coding. The machine learning surrogate models inherit the advantages the physical-based ASLUM v4.1 model in terms of core dynamics, accuracy, and high resolution, with enhanced computational efficiency and user-friendliness to practitioners. Based on scenario comparison and optimization under constraints, specific mitigation strategies can be derived for both existing and developing urban areas. The versatility of the proposed method and its further improvement (e.g., web-based and graphic user interface development) will help to foster decision making processes and enable policy makers and urban planners to gain deeper and more holistic insight into sustainable solutions that promotes the overall livability of cities.

The transition from complex process-based modeling to ML-based protocols, albeit at its infancy, is transformative and has the potential to furnish a new paradigm in urban system modeling using advanced computer techniques, and further our fundamental understanding of the complex urban ecosystem and the interactions among its diverse components. Future work is planned to take the full advantage of data-driven techniques to form comprehensive and systematic views of compound urban environmental assessment including UHI, building energy efficiency, ecosystem services, air quality, anthropogenic CO_2 emission, etc.

Acknowledgement

This study is based upon work supported by the U.S. National Science Foundation (NSF) under grants AGS-1930629, CBET-2028868, GEO-2044051, and CISE-1931297, the National Aeronautics and Space Administration (NASA) under grant # 80NSSC20K1263, and National Oceanic and Atmospheric Administration (NOAA) under grant NA20OAR4310341. We also acknowledge the Central Arizona-Phoenix Long-Term Ecological Research (CAP LTER) project under NSF grant # DEB-1637590 for providing the field measurement. Data used in this study is available at https://sustainability.asu.edu/caplter/research/long-term-monitoring/urban-flux-tower/.

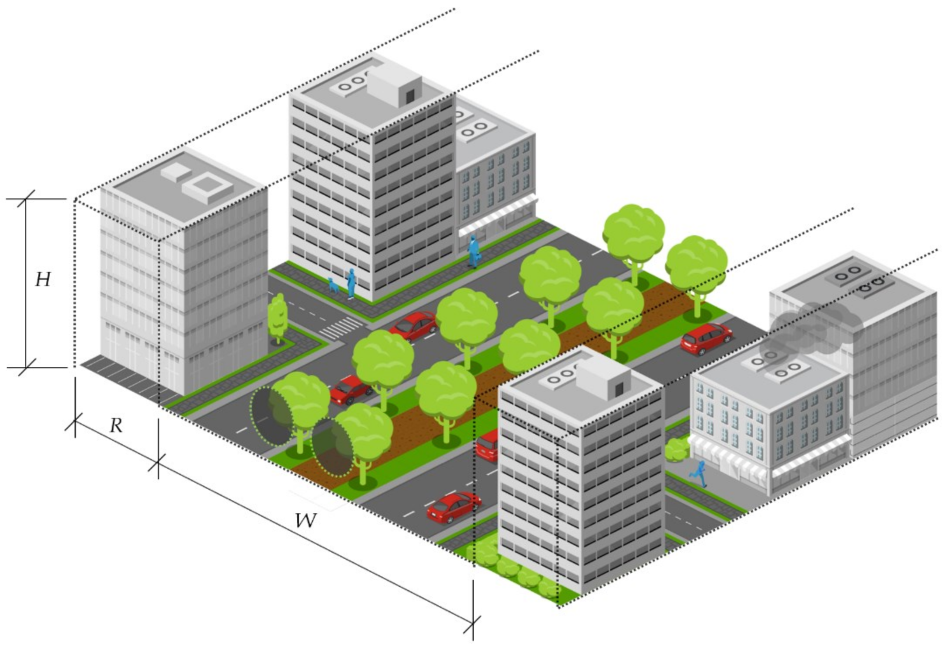

Figure 1. Schematic of urban representation in a single layer urban canopy model. *H*, *R* and *W* represent normalized building height, width of building portion and non-building portion, respectively. A street canyon includes two symmetric rows of street trees, specified by tree height (h_T), crown radius (r_T), and tree location (c_T). Non-building portion is further configured as paved (dark gray), lawn (dark green), and bare soil surfaces (brown). CO_2 exchanges include anthropogenic emissions from building (light gray), human (blue), and vehicle (red) and biogenic exchanges from tree (light green), lawn (dark green), and bare soil (brown).

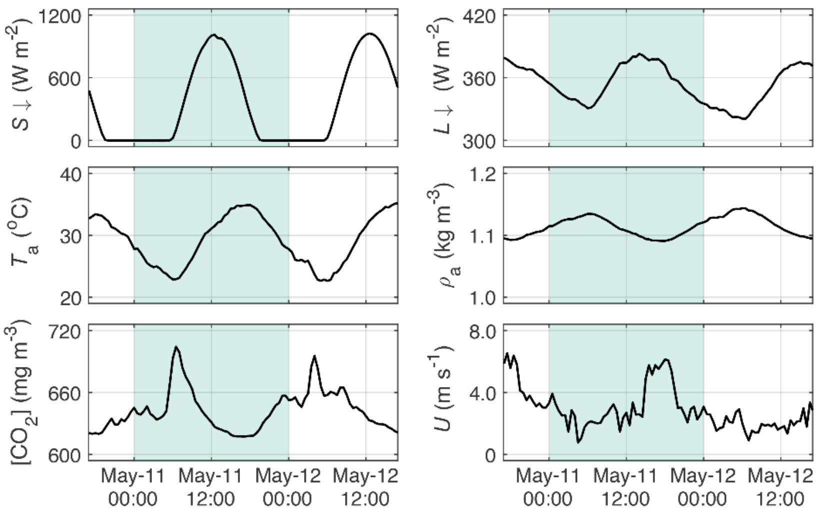

Figure 2. Meteorological forcing used in the simulation (a) downwelling shortwave ($S\downarrow$) and longwave ($L\downarrow$) radiations; (b) air temperature (T_a) and windspeed (U); (c) background CO_2 concentration ([CO_2]) and air density (ρ_a). Mean T_{can} and NEE are calculated during the shaded period (24 hours). Results from non-shaded period are used for quality control in ASLUM and are not used in ML training and test.

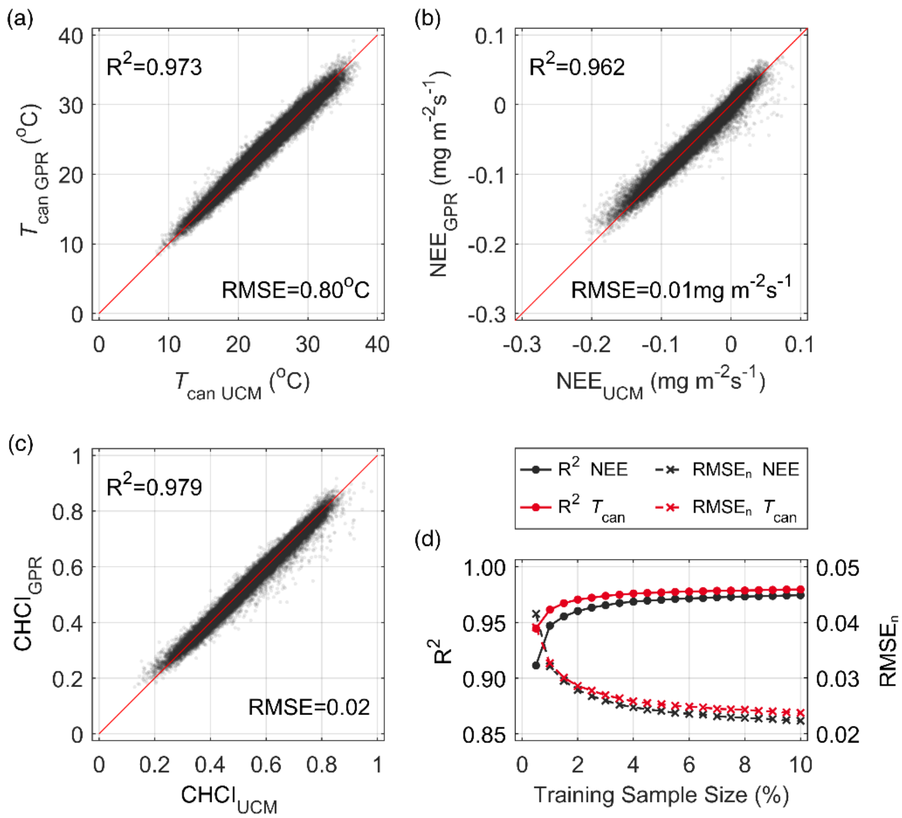

502

503 **Figure 3**. Performance of ML training and tests using the GPR surrogate for (a) T_{can}, (b) NEE, 504 (c) CHCI when trained using 5% of the simulated dataset, and (d) the ensemble mean of R^2 and 505 normalized RMSE ($RMSE_n$) of T_{can} and NEE when trained using different training sample sizes. 506 For each sample size, model performance is evaluated as the average of 20 replicate runs.

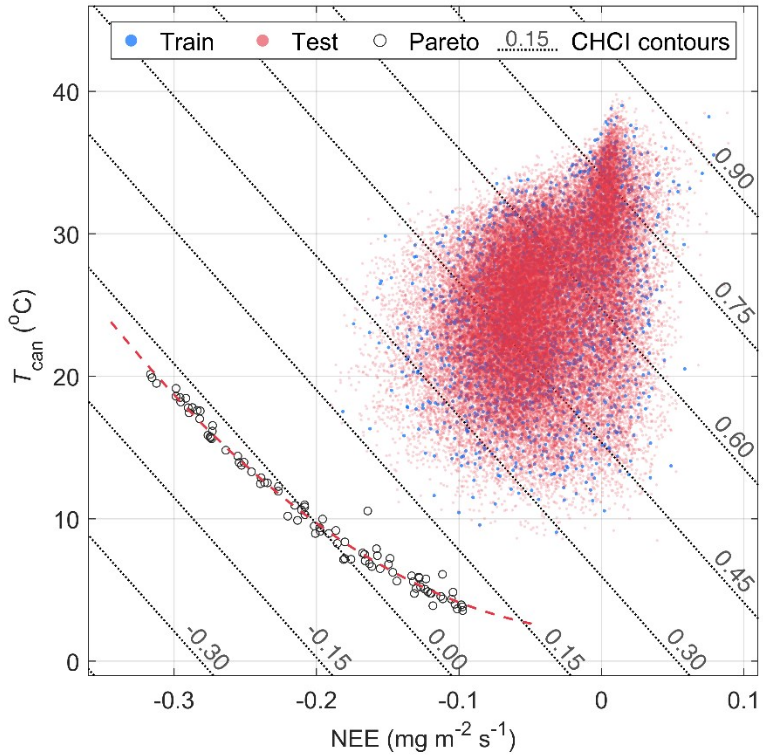

Figure 4. Scatter plots of the original dataset and the Pareto solutions found via GA multi-objective optimization. The red dashed line indicates the Pareto front formed by Pareto solutions. The dotted lines in the background indicate the contours of CHCI.

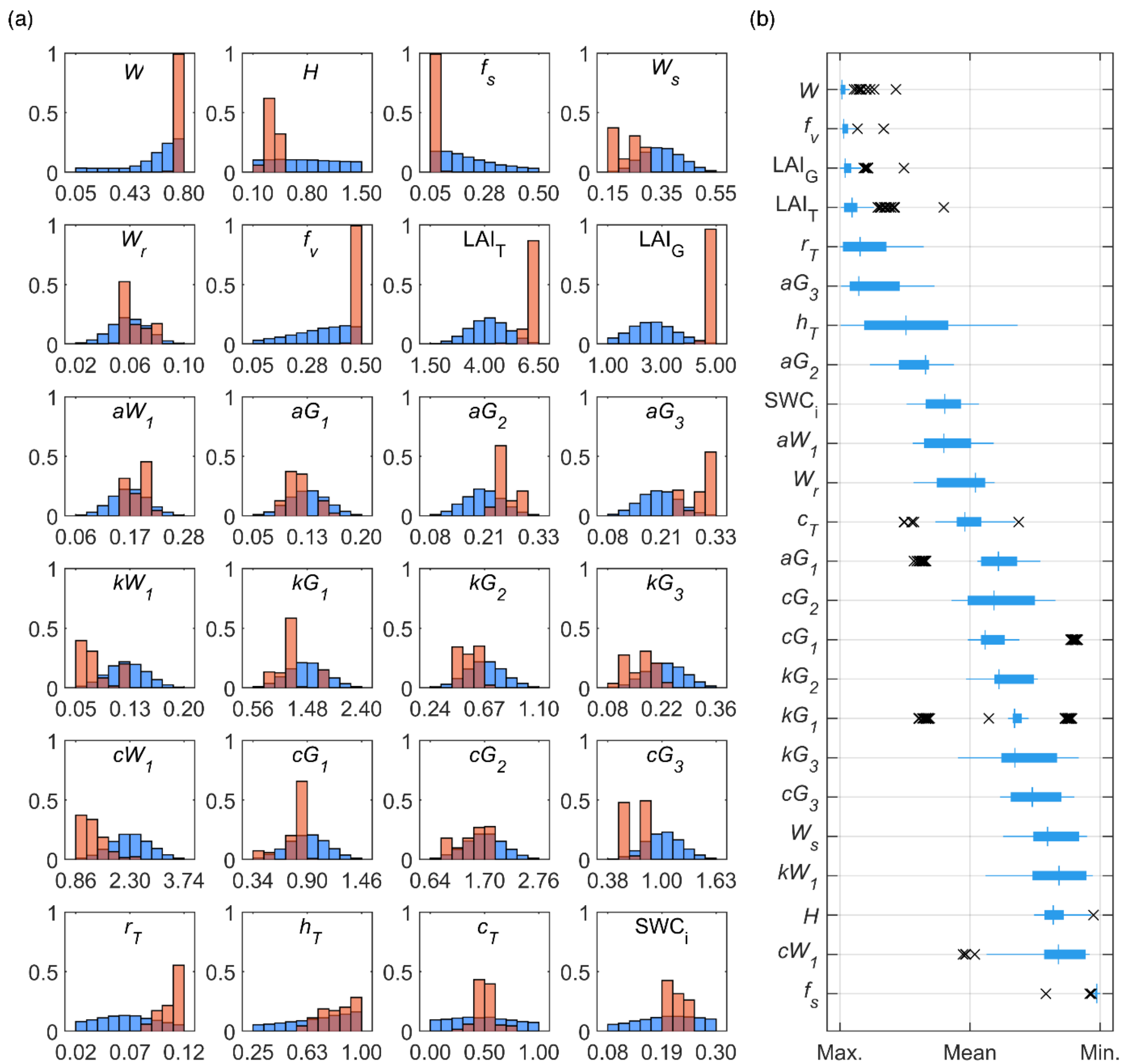

Figure 5. (a) Histograms (normalized to probability) of 24 urban features in original dataset (blue) and Pareto solutions (orange), and (b) boxplot of the parameters that lead to Pareto solutions. Values are normalized by Eq. (7). Max. Mean and Min. represent the numerical range of urban features in Table 1.

Table 1. Variables used as training features for Gaussian Process regression models.

Name	Unit	Mean	Std.	Min.	Max.
Canyon geometry					
Normalized road width					
W	-	0.60	0.19	0.05	0.80
Normalized building height					
H	-	0.78	0.40	0.10	1.50
Soil properties					
Bare soil fraction					
f_s	-	0.21	0.11	0.05	0.50
Saturation soil moisture					
W_s	-	0.35	0.07	0.15	0.55
Residual soil moisture					
W_r	-	0.06	0.01	0.02	0.10
Initial soil moisture					
SWC_i	-	0.20	0.06	0.08	0.30
Plant properties					
Lawn fraction					
f_v	-	0.33	0.11	0.05	0.50
Tree - Leaf area index					
LAI_T	m^2/m^2	4.15	0.87	1.50	6.50
Grass - Leaf area index					
LAI_G	m^2/m^2	2.68	0.79	1.00	5.00
Tree crown size					
r_T	-	0.07	0.03	0.02	0.12
Tree height					
h_T	-	0.70	0.21	0.25	1.00
Tree location					
c_T	-	0.48	0.27	0.00	1.00

Name	Unit	Mean	Std.	Min.	Max.
Material properties					
Albedo - Wall					
aW_1	-	0.17	0.04	0.06	0.28
Albedo - Paved					
aG_1	-	0.13	0.03	0.05	0.20
Albedo - Lawn					
aG_2	-	0.20	0.04	0.08	0.33
Albedo - Bare soil					
aG_3	-	0.20	0.04	0.08	0.33
Thermal conductivity - Wall					
kW_1	$Wm^{-1}K^{-1}$	0.12	0.03	0.05	0.20
Thermal conductivity - Paved					
kG_1	$Wm^{-1}K^{-1}$	1.49	0.33	0.56	2.44
Thermal conductivity - Lawn					
kG_2	$Wm^{-1}K^{-1}$	0.65	0.14	0.24	1.06
Thermal conductivity - Bare soil					
kG_3	$Wm^{-1}K^{-1}$	0.23	0.05	0.08	0.36
Heat capacity - Wall					
cW_1	$MJm^{-3}\,K^{-1}$	2.31	0.51	0.86	3.74
Heat capacity - Paved					
cG_1	$MJm^{-3}\,K^{-1}$	0.90	0.20	0.34	1.46
Heat capacity - Lawn					
cG_2	$MJm^{-3}\,K^{-1}$	1.70	0.37	0.64	2.76
Heat capacity - Bare soil					
cG_3	$MJm^{-3}\,K^{-1}$	1.02	0.21	0.38	1.63

Reference

Abdel-Ghany, A. M., Al-Helal, I. M., & Shady, M. R. (2013). Human thermal comfort and heat stress in an outdoor urban arid environment: A case study. *Advances in Meteorology, 2013*, 693541. http://doi.org/10.1155/2013/693541

Akbari, H. (2002). Shade trees reduce building energy use and CO_2 emissions from power plants. *Environmental Pollution, 116*, S119-S126. http://doi.org/10.1016/S0269-7491(01)00264-0

Akhtar, T., & Shoemaker, C. A. (2016). Multi objective optimization of computationally expensive multi-modal functions with RBF surrogates and multi-rule selection. *Journal of Global Optimization, 64*(1), 17-32. http://doi.org/10.1007/s10898-015-0270-y

Amini Parsa, V., Salehi, E., Yavari, A. R., & van Bodegom, P. M. (2019). Evaluating the potential contribution of urban ecosystem service to climate change mitigation. *Urban Ecosystems, 22*(5), 989-1006. http://doi.org/10.1007/s11252-019-00870-w

Aram, F., Higueras García, E., Solgi, E., & Mansournia, S. (2019). Urban green space cooling effect in cities. *Heliyon, 5*(4), e01339. http://doi.org/10.1016/j.heliyon.2019.e01339

Baruti, M. M., Johansson, E., & Åstrand, J. (2019). Review of studies on outdoor thermal comfort in warm humid climates: challenges of informal urban fabric. *International Journal of Biometeorology, 63*(10), 1449-1462. http://doi.org/10.1007/s00484-019-01757-3

Barwise, Y., & Kumar, P. (2020). Designing vegetation barriers for urban air pollution abatement: a practical review for appropriate plant species selection. *Climate and Atmospheric Science, 3*(1), 12. http://doi.org/10.1038/s41612-020-0115-3

Bazaz, A., Bertoldi, P., Buckeridge, M., Cartwright, A., de Coninck, H., Engelbrecht, F., … & Waisman, H. (2018). Summary for urban policymakers: What the IPCC special report on 1.5ºC means for cities. de Coninck, H., Klaus, I., Revi, A., Schultz, S., Solecki, W. eds. 30 pp. http://doi.org/10.24943/SCPM.2018

Bessa, M.A., Bostanabad, R., Liu, Z., Hu, A., Apley, D. W., Brinson, C., Chen, W. & Liu, W. K. (2017) A framework for data-driven analysis of materials under uncertainty: countering the curse of dimensionality. *Computer Methods in Applied Mechanics Engeering*, 320, 633–667. https://doi.org/10.1016/j.cma.2017.03.037.

Cai, X., Zeng, R., Kang, W. H., Song, J., & Valocchi, A. J. (2015). Strategic Planning for Drought Mitigation under Climate Change. *Journal of Water Resources Planning and Management, 141*(9), 04015004. http://doi.org/10.1061/(ASCE)WR.1943-5452.0000510

Camps-Valls, G., Martino, L., Svendsen, D. H., Campos-Taberner, M., Muñoz-Marí, J., Laparra, V., . . . García-Haro, F. J. (2018). Physics-aware Gaussian processes in remote sensing. *Applied Soft Computing, 68*, 69-82. http://doi.org/10.1016/j.asoc.2018.03.021

Chen, W. Y. (2015). The role of urban green infrastructure in offsetting carbon emissions in 35 major Chinese cities: A nationwide estimate. *Cities, 44*, 112-120. http://doi.org/10.1016/j.cities.2015.01.005

Chow, W. T. L., Volo, T. J., Vivoni, E. R., Jenerette, G. D., & Ruddell, B. L. (2014). Seasonal dynamics of a suburban energy balance in Phoenix, Arizona. *International Journal of Climatology, 34*(15), 3863-3880. http://doi.org/10.1002/joc.3947

Chow, W. T. L. (2017). Eddy covariance data measured at the CAP LTER flux tower located in the west Phoenix, AZ neighborhood of Maryvale from 2011-12-16 through 2012-12-31 ver 1. *Environmental Data Initiative*. Accessed 2021-07-02. https://doi.org/10.6073/pasta/fed17d67583eda16c439216ca40b0669

Creutzig, F., Lohrey, S., Bai, X., Baklanov, A., Dawson, R., Dhakal, S., . . . Walsh, B. (2019). Upscaling urban data science for global climate solutions. *Global Sustainability, 2*, e2. http://doi.org/10.1017/sus.2018.16

Deb, K. (2001). Multi-Objective optimization using evolutionary algorithms. Chichester, England: John Wiley & Sons, 2001

Diwekar, U. M. (2020). Optimization under uncertainty. In *Introduction to Applied Optimization*. pp. 151-215. Boston, MA: Springer US.

Escobedo, F., Varela, S., Zhao, M., Wagner, J. E., & Zipperer, W. (2010). Analyzing the efficacy of subtropical urban forests in offsetting carbon emissions from cities. Environmental Science & Policy 13:362-372.

Executable Books Community (2020) Jupyter Book (Version v0.10). Zenodo. http://doi.org/10.5281/zenodo.4539666

Fang, D., Zhang, X., Yu, Q., Jin, T. C., & Tian, L. (2018). A novel method for carbon dioxide emission forecasting based on improved Gaussian processes regression. *Journal of Cleaner Production, 173*, 143-150. http://doi.org/10.1016/j.jclepro.2017.05.102

Gao, M., Chen, F., Shen, H., & Li, H. (2020). A tale of two cities: different urban heat mitigation efficacy with the same strategies. *Theoretical and Applied Climatology, 142*(3), 1625-1640. http://doi.org/10.1007/s00704-020-03390-2

Gettelman, A., Gagne, D. J., Chen, C.-C., Christensen, M. W., Lebo, Z. J., Morrison, H., & Gantos, G. (2021). Machine learning the warm rain process. *Journal of Advances in Modeling Earth Systems, 13*(2), e2020MS002268. http://doi.org/10.1029/2020MS002268

Gobakis, K., Kolokotsa, D., Synnefa, A., Saliari, M., Giannopoulou, K., & Santamouris, M. (2011). Development of a model for urban heat island prediction using neural network techniques. *Sustainable Cities and Society, 1*(2), 104-115. http://doi.org/10.1016/j.scs.2011.05.001

Goret, M., Masson, V., Schoetter, R., & Moine, M.-P. (2019). Inclusion of CO_2 flux modelling in an urban canopy layer model and an evaluation over an old European city centre. *Atmospheric Environment: X, 3*, 100042. http://doi.org/10.1016/j.aeaoa.2019.100042

He, W., Zeng, Y., & Li, G. (2020). An adaptive polynomial chaos expansion for high-dimensional reliability analysis. *Structural and Multidisciplinary Optimization, 62*(4), 2051-2067. http://doi.org/10.1007/s00158-020-02594-4

IPCC (2014). Climate Change 2014: Synthesis Report. Contribution of Working Groups I, II and III to the Fifth Assessment Report of the Intergovernmental Panel on Climate Change. R.K. Pachauri and L.A. Meyer (eds.) IPCC, Geneva, Switzerland, 151 pp.

Järvi, L., Nordbo, A., Junninen, H., Riikonen, A., Moilanen, J., Nikinmaa, E., & Vesala, T. (2012). Seasonal and annual variation of carbon dioxide surface fluxes in Helsinki, Finland, in 2006–2010. *Atmos. Chem. Phys., 12*(18), 8475-8489. http://doi.org/10.5194/acp-12-8475-2012

Kim, S. H., & Boukouvala, F. (2020). Machine learning-based surrogate modeling for data-driven optimization: a comparison of subset selection for regression techniques. *Optimization Letters, 14*(4), 989-1010. http://doi.org/10.1007/s11590-019-01428-7

Lai, D., Liu, W., Gan, T., Liu, K., & Chen, Q. (2019). A review of mitigating strategies to improve the thermal environment and thermal comfort in urban outdoor spaces. *Science of The Total Environment, 661*, 337-353. http://doi.org/10.1016/j.scitotenv.2019.01.062

Laloy, E., & Jacques, D. (2019). Emulation of CPU-demanding reactive transport models: a comparison of Gaussian processes, polynomial chaos expansion, and deep neural networks. *Computational Geosciences, 23*(5), 1193-1215. http://doi.org/10.1007/s10596-019-09875-y

Lemonsu, A., Masson, V., Shashua-Bar, L., Erell, E., & Pearlmutter, D. (2012). Inclusion of vegetation in the Town Energy Balance model for modelling urban green areas. *Geosci. Model Dev., 5*(6), 1377-1393. http://doi.org/10.5194/gmd-5-1377-2012

Li, P., & Wang, Z.-H. (2020). Modeling carbon dioxide exchange in a single-layer urban canopy model. *Building and Environment, 184*, 107243. http://doi.org/10.1016/j.buildenv.2020.107243

Li, P., & Wang, Z.-H. (2021a). Environmental co-benefits of urban greening for mitigating heat and carbon emissions. *Journal of Environmental Management, 293*, 112963. http://doi.org/10.1016/j.jenvman.2021.112963

Li, P., & Wang, Z.-H. (2021b). Uncertainty and sensitivity analysis of modeling plant CO_2 exchange in the built environment. *Building and Environment, 189*, 107539. http://doi.org/10.1016/j.buildenv.2020.107539

Masson, V. (2000). A Physically-Based Scheme For The Urban Energy Budget In Atmospheric Models. *Boundary-Layer Meteorology, 94*(3), 357-397. http://doi.org/10.1023/A:1002463829265

McCall, J. (2005). Genetic algorithms for modelling and optimisation. *Journal of Computational and Applied Mathematics*.*184*(1):205–22. https://doi.org/10.1016/j.cam.2004.07.034

McDonald, D. B., Grantham, W. J., Tabor, W. L., & Murphy, M. J. (2007). Global and local optimization using radial basis function response surface models. *Applied Mathematical Modelling, 31*(10), 2095-2110. http://doi.org/doi.org/10.1016/j.apm.2006.08.008

Meili, N., Manoli, G., Burlando, P., Bou-Zeid, E., Chow, W. T. L., Coutts, A. M., . . . Fatichi, S. (2020). An urban ecohydrological model to quantify the effect of vegetation on urban climate and hydrology (UT&C v1.0). *Geosci. Model Dev., 13*(1), 335-362. http://doi.org/10.5194/gmd-13-335-2020

Milojevic-Dupont, N., & Creutzig, F. (2021). Machine learning for geographically differentiated climate change mitigation in urban areas. *Sustainable Cities and Society, 64*, 102526. http://doi.org/10.1016/j.scs.2020.102526

Mishra, A. A., Mukhopadhaya, J., Alonso, J., & Iaccarino, G. (2020). Design exploration and optimization under uncertainty. *Physics of Fluids, 32*(8), 085106. http://doi.org/10.1063/5.0020858

Ngatchou, P., Zarei, A., & El-Sharkawi, A. (2005, 6-10 Nov. 2005). *Pareto multi-objective optimization.* Paper presented at the Proceedings of the 13th International Conference on, Intelligent Systems Application to Power Systems.

Oh, J. W., Ngarambe, J., Duhirwe, P. N., Yun, G. Y., & Santamouris, M. (2020). Using deep-learning to forecast the magnitude and characteristics of urban heat island in Seoul Korea. *Scientific Reports, 10*(1), 3559. http://doi.org/10.1038/s41598-020-60632-z

Oke, T. R. (1973). City size and the urban heat island. *Atmospheric Environment (1967), 7*(8), 769-779. http://doi.org/10.1016/0004-6981(73)90140-6

Oke, T. R. (1981). Canyon geometry and the nocturnal urban heat island: Comparison of scale model and field observations. *Journal of Climatology, 1*(3), 237-254. http://doi.org/10.1002/joc.3370010304

Pena Acosta, M., Vahdatikhaki, F., Santos, J., Hammad, A., & Dorée, A. G. (2021). How to bring UHI to the urban planning table? A data-driven modeling approach. *Sustainable Cities and Society, 71*, 102948. http://doi.org/10.1016/j.scs.2021.102948

Rasmussen, C.E. and Williams, C.K.I. (2006). Gaussian processes for ine learning. The MIT Press.

Razavi, S., Tolson, B. A., & Burn, D. H. (2012). Numerical assessment of metamodelling strategies in computationally intensive optimization. *Environmental Modelling & Software, 34*, 67-86. http://doi.org/10.1016/j.envsoft.2011.09.010

Riondato, E., Pilla, F., Sarkar Basu, A., & Basu, B. (2020). Investigating the effect of trees on urban quality in Dublin by combining air monitoring with i-Tree Eco model. *Sustainable Cities and Society, 61*, 102356. http://doi.org/10.1016/j.scs.2020.102356

Rosenzweig, C., Solecki, W., Hammer, S. A., & Mehrotra, S. (2010). Cities lead the way in climate–change action. *Nature, 467*(7318), 909-911. http://doi.org/10.1038/467909a

Ryu, Y.-H., Bou-Zeid, E., Wang, Z.-H., & Smith, J. A. (2016). Realistic representation of trees in an urban canopy model. *Boundary-Layer Meteorology, 159*(2), 193-220. http://doi.org/10.1007/s10546-015-0120-y

Skala, V. (2017). RBF interpolation with CSRBF of large data sets. *Procedia Computer Science, 108*, 2433-2437. http://doi.org/10.1016/j.procs.2017.05.081

Skamarock, W. C., Klemp, J. B., Dudhia, J., Gill, D. O., Liu, Z., Berner, J., Wang, W., Powers, J. G., Duda, M. G., Barker, D. M., & Huang, X.-Y. (2019). A Description of the Advanced

Research WRF Version 4. NCAR Tech. Note NCAR/TN-556+STR, 145 pp. http://doi.org/10.5065/1dfh-6p97

Song, J., & Wang, Z.H. (2015). Impacts of mesic and xeric urban vegetation on outdoor thermal comfort and microclimate in Phoenix, AZ. *Building and Environment*, *94*(2), 558-568. https://doi.org/10.1016/j.buildenv.2015.10.016

Song, J., Wang, Z.-H., & Wang, C. (2017). Biospheric and anthropogenic contributors to atmospheric CO_2 variability in a residential neighborhood of Phoenix, Arizona. *Journal of Geophysical Research: Atmospheres, 122*(6), 3317-3329. http://doi.org/10.1002/2016JD026267

Stavropulos-Laffaille, X., Chancibault, K., Brun, J. M., Lemonsu, A., Masson, V., Boone, A., & Andrieu, H. (2018). Improvements to the hydrological processes of the Town Energy Balance model (TEB-Veg, SURFEX v7.3) for urban modelling and impact assessment. *Geosci. Model Dev., 11*(10), 4175-4194. http://doi.org/10.5194/gmd-11-4175-2018

Strohbach, M. W., Arnold, E., & Haase, D. (2012). The carbon footprint of urban green spaces: A life cycle approach. *Landscape and Urban Planning, 104*(2), 220-229. http://doi.org/10.1016/j.landurbplan.2011.10.013

Sun, T., & Grimmond, S. (2019). A Python-enhanced urban land surface model SuPy (SUEWS in Python, v2019.2): development, deployment and demonstration. *Geosci. Model Dev., 12*(7), 2781-2795. http://doi.org/10.5194/gmd-12-2781-2019

United Nations Framework Convention on Climate Change (2015). Paris Agreement. Retrieved from https://unfccc.int/process/conferences/pastconferences/paris-climate-change-conference-november-2015/paris-agreement

United Nations Framework Convention on Climate Change (2020). Number of global cities recognized for climate leadership doubles. Retrieved from https://unfccc.int/news/number-of-global-cities-recognized-for-climate-leadership-doubles

Upreti, R., Wang, Z.H., & Yang, J. (2017). Radiative shading effect of urban trees on cooling the regional built environment. *Urban Forestry & Urban Greening*, *26*, 18-24. https://doi.org/10.1016/j.ufug.2017.05.008

Velasco, E., Roth, M., Norford, L., & Molina, L. T. (2016). Does urban vegetation enhance carbon sequestration? *Landscape and Urban Planning, 148*, 99-107. http://doi.org/10.1016/j.landurbplan.2015.12.003

Vivoni, E. R., Kindler, M., Wang, Z., & Pérez-Ruiz, E. R. (2020). Abiotic mechanisms drive enhanced evaporative losses under urban oasis conditions. *Geophysical Research Letters, 47*(22), e2020GL090123. http://doi.org/10.1029/2020GL090123

Wang, C., Wang, Z.-H., & Ryu, Y.-H. (2021a). A single-layer urban canopy model with transmissive radiation exchange between trees and street canyons. *Building and Environment, 191*, 107593. http://doi.org/10.1016/j.buildenv.2021.107593

Wang, C., Wang, Z.H., Kaloush, K.E., & Shacat, J. (2021b). Cool pavements for urban heat island mitigation: A synthetic review. *Renewable & Sustainable Energy Reviews*, *146*, 111171. https://doi.org/10.1016/j.rser.2021.111171

Wang, C., Wang, Z.-H., Wang, C., & Myint, S. W. (2019). Environmental cooling provided by urban trees under extreme heat and cold waves in U.S. cities. *Remote Sensing of Environment, 227*, 28-43. http://doi.org/10.1016/j.rse.2019.03.024

Wang, C., Wang, Z.-H., & Yang, J. (2018). Cooling effect of urban trees on the built environment of contiguous United States. *Earth's Future, 6*(8), 1066-1081. http://doi.org/10.1029/2018EF000891

Wang, Z.-H., Bou-Zeid, E., Au, S. K., & Smith, J. A. (2011). Analyzing the sensitivity of WRF's single-layer urban canopy model to parameter uncertainty using advanced Monte Carlo simulation. *Journal of Applied Meteorology and Climatology*, 50(9), 1795-1814. https://doi.org/10.1175/2011jamc2685.1

Wang, Z.-H., Bou-Zeid, E., & Smith, J. A. (2013). A coupled energy transport and hydrological model for urban canopies evaluated using a wireless sensor network. *Quarterly Journal of the Royal Meteorological Society, 139*(675), 1643-1657. http://doi.org/10.1002/qj.2032

Wang, Z.-H. (2014). Monte Carlo simulations of radiative heat exchange in a street canyon with trees. *Solar Energy*, *110*, 704-713. https://doi.org/10.1016/j.solener.2014.10.012

Wang, Z.-H., Zhao, X., Yang, J., & Song, J. (2016). Cooling and energy saving potentials of shade trees and urban lawns in a desert city. *Applied Energy*, *161*(3), 437-444. https://doi.org/10.1016/j.apenergy.2015.10.047

Ward, H. C., Kotthaus, S., Grimmond, C. S. B., Bjorkegren, A., Wilkinson, M., Morrison, W. T. J., . . . Iamarino, M. (2015). Effects of urban density on carbon dioxide exchanges: Observations of dense urban, suburban and woodland areas of southern England. *Environmental Pollution, 198*, 186-200. http://doi.org/10.1016/j.envpol.2014.12.031

Weissert, L. F., Salmond, J. A., & Schwendenmann, L. (2014). A review of the current progress in quantifying the potential of urban forests to mitigate urban CO_2 emissions. *Urban Climate, 8*, 100-125. http://doi.org/10.1016/j.uclim.2014.01.002

Wong, N. H., Tan, C. L., Kolokotsa, D. D., & Takebayashi, H. (2021). Greenery as a mitigation and adaptation strategy to urban heat. *Nature Reviews Earth & Environment, 2*(3), 166-181. http://doi.org/10.1038/s43017-020-00129-5

Xu, T., & Liang, F. (2021). Machine learning for hydrologic sciences: An introductory overview. *WIREs Water, n/a*(n/a), e1533. http://doi.org/10.1002/wat2.1533

Yang, J., & Wang, Z.-H. (2014). Physical parameterization and sensitivity of urban hydrological models: Application to green roof systems. *Building and Environment, 75*, 250-263. http://doi.org/10.1016/j.buildenv.2014.02.006

Yang, J., Wang, Z.-H., Chen, F., Miao, S., Tewari, M., Voogt, J. A., & Myint, S. (2015a). Enhancing hydrologic modelling in the coupled Weather Research and Forecasting–Urban Modelling system. *Boundary-Layer Meteorology, 155*(1), 87-109. http://doi.org/10.1007/s10546-014-9991-6

Yang, J., Wang, Z.H., & Kaloush, K.E. (2015b). Environmental impacts of reflective materials: Is high albedo a 'silver bullet' for mitigating urban heat island? *Renewable and Sustainable Energy Reviews*, *47*, 830-843. https://doi.org/10.1010/j.rser.2015.03.092

Yang, J., Wang, Z.-H., Kaloush, K. E., & Dylla, H. (2016). Effect of pavement thermal properties on mitigating urban heat islands: A multi-scale modeling case study in Phoenix. *Building and Environment, 108*, 110-121. http://doi.org/10.1016/j.buildenv.2016.08.021

Yang, J., & Wang, Z.H. (2017). Planning for a sustainable desert city: The potential water buffering capacity of urban green infrastructure. *Landscape and Urban Planning*, *167*, 339-347. https://doi.org/10.1016/j.landurbplan.2017.07.014

Zhang, X., Yan, F., Liu, H., & Qiao, Z. (2021). Towards low carbon cities: A machine learning method for predicting urban blocks carbon emissions (UBCE) based on built environment factors (BEF) in Changxing City, China. *Sustainable Cities and Society, 69*, 102875. http://doi.org/10.1016/j.scs.2021.102875